Monolithic Fabrication of EWOD Chips for Picoliter Droplets

Wyatt C. Nelson and Chang-Jin "CJ" Kim, *Member, IEEE, Fellow, ASME*

***Abstract*—We report monolithic fabrication of parallel-plate electrowetting-on-dielectric (EWOD) chips for digital microfluidics of picoliter droplets. Instead of assembling a second substrate to form a top plate—the common practice with all previous parallel-plate EWOD chips—the top plate is surface micromachined as a transparent thin-film membrane that forms a monolithic cavity having a gap height on the order of micrometers with excellent accuracy and uniformity. The membrane is embedded with EWOD driving electrodes and confines droplets against the device substrate to perform digital microfluidic operations. Two main attributes of the monolithic architecture that distinguish it from tradition methods are: (i) it enables excellent control of droplet dimensions down to the micrometer scale, and (ii) it does not require the typical alignment and assembly steps. Basic device functions such as creation and splitting are verified by EWOD actuation of ∼100 picoliter droplets surrounded by air or oil inside a 10 μm-high cavity. Additionally, flow focusing of droplets containing 5.3 μm beads demonstrates one example of the utilities afforded by monolithic fabrication. [2011-0148]**

***Index Terms*—Digital microfluidics, electrowetting, electrowetting-on-dielectric (EWOD), monolithic fabrication, picoliter droplets.**

I. Introduction

FOR VARIOUS reasons [1], we have yet to see the broad implementation of microfluidic systems as automated bioanalytical tools. For example, the benefits of miniaturization through microfluidics (e.g., fast reaction times, low waste, and high sensitivity detection) are usually not attained without trained technicians and a specialized assortment of benchtop components, often including mechanical pumps and valve manifolds. In this light, digital microfluidic[1] [2], [3] systems based on electrowetting are attractive because they enable fluid actuation by electrical signals alone, thereby reducing the complexity of the chip as well as the overall system. Such electrically driven microfluidics, particularly using the chip configuration of electrowetting-on-dielectric (EWOD) [4], have shown promise as "generic platforms," because they can be reprogrammed on-the-fly using software to accommodate various biochemical protocols. Further, because EWOD chips have low power requirements, it is conceivable to build a handheld (e.g., cellphone-like) system that runs on batteries [5].

Most EWOD-based digital microfluidic devices have one of the following generic architectures: parallel-plate [6], [7] or open-planar [8], [9]. Of these, the former is often preferred, despite the additional steps in fabrication, for its utility and reliability in applications. For example, it is far easier to generate droplets and split them apart when a liquid is squeezed between two plates. Also, controlling the device gap (between the plates) is a reliable way to scale the working fluid. In comparison, on an open-planar device, droplet dimensions are determined by the contact angle, which is nearly impossible to control or predict with accuracy. Third, if the gap is much smaller than the capillary length (e.g., 2–3 mm for water), large droplets are insensitive to inertial forces. The same cannot be said for open-planar devices unless the droplet volume is small, i.e., the diameter is much smaller than the capillary length.

Traditional parallel-plate EWOD device manufacturing begins with thin film deposition and patterning of the two plates—typically a bottom substrate patterned with EWOD electrodes and a top plate with a blank conductive layer—and ends with assembly. Overall, the plates are simple to fabricate in the clean room, for example, using one step each of metallization, photolithography, and dielectric deposition. The assembly process, which can be performed using a variety of methods, involves alignment of the two plates (which is not critical for most applications because the ground plate is unpatterned), fabricating and positioning spacers, and bonding of the plates; the last two steps determine the gap between the plates and therefore the thickness of the droplets. In research laboratories, it is common to align and affix cutouts of an adhesive spacer, e.g., double-sided tape, to the plates for spacing and bonding. This practice is acceptable for fabricating parallel-plate EWOD devices with relatively large gaps (i.e., > 50 μm). When smaller gaps are desired, a thick photoresist (e.g., SU-8) can be coated and lithographically defined as a spacer, and additional provisions, e.g., external alignment and clamping mechanisms, are employed to hold the plates together. Song *et al.* [10], Lin *et al.* [11], and Welch *et al.* [12] have demonstrated excellent performance using such devices for handling droplets as small as 35 pL in oil. Welch *et al.* [12] have also demonstrated how problems associated with slight irregularities in

Manuscript received May 10, 2011; revised July 18, 2011; accepted August 12, 2011. Date of publication October 6, 2011; date of current version December 2, 2011. This work was supported by an NSF Integrative Graduate Education and Research Traineeship (DGE-0654431) through the UCLA Materials Creation Training Program (MCTP) and the NSF Graduate Research Fellowship Program (DGE-0707424). Subject Editor Y. Zohar.

The authors are with the Mechanical and Aerospace Engineering Department, University of California at Los Angeles (UCLA), Los Angeles, CA 90095-1597 USA (e-mail: wyattnelson@ucla.edu; cjkim@seas.ucla.edu).

Color versions of one or more of the figures in this paper are available online at http://ieeexplore.ieee.org.

Digital Object Identifier 10.1109/JMEMS.2011.2167673

[1]"Digital" in digital microfluidics implies that droplets are manipulated individually, i.e., each can be controlled independently. In this definition [2], [3], droplets manipulated as a group (e.g., multiple droplets moving with a carrier fluid pumped in a microchannel) would belong to droplet microfluidics but not necessarily digital.

the thickness of spin-on spacers can be alleviated by using an additional polymer layer on the top plate. Note, however, that a spin-coated polymeric spacer would not provide the levels of uniformity and repeatability in the gap dimension that are readily achievable using surface micromachining methods based on common integrated circuit processes, e.g., oxidation of silicon, chemical vapor deposition.

This paper explains our recent progress in developing a concept initially proposed in [13], in which we demonstrated EWOD actuation of $\sim$100 pL droplets immersed in oil in a monolithically fabricated parallel-plate device. Having refined the design and fabrication processes, our newest results include repeatable EWOD-driven creation, transportation, splitting, and merging of $\sim$100 pL droplets in air as well as oil. Our purpose in developing a surface-micromachined parallel-plate EWOD chip is not to replace traditional chips; instead, we are interested in exploring a new process because it brings new opportunities. In fact, since the proposed micromachining processes is much more involved than typical EWOD device fabrication, the latter will undoubtedly be preferred in applications for which it makes sense, e.g., large-gap devices. The main attributes of our surface micromachining processes that distinguish it from traditional methods are: (i) it enables excellent control of droplet dimensions down to the micrometer, scale and (ii) it does not require alignment and assembly steps.

Since it requires special fabrication techniques to repeatedly form accurate gaps smaller than ~ 50 μm, most reported parallel-plate EWOD chips are designed to handle droplets greater than $\sim$100 nL (i.e., 1000 μm $\times$ 1000 μm $\times$ 100 μm; note that a water droplet needs to be at least five times wider than its thickness to allow for all the basic digital microfluidic operations in air, i.e., without filling the gap with oil [7]). The gap heights of the reported monolithic chips are set by the thickness of the sacrificial layer, which is the device layer of a silicon-on-insulator (SOI) wafer and guaranteed by the manufacturer (Ultrasil) to ± 0.5 μm across the wafer. We chose to use SOI wafers to obtain a relatively thick sacrificial layer (i.e., 10 μm used in this study); one would deposit a thin film for a thin sacrificial layer (e.g., 1 μm). With such accuracy in the gap, the minimum droplet volume in the monolithic chip is determined by the lithography of the EWOD electrodes. Using electrodes 100 μm on a side with a 10 μm distance between them and a 10 μm-thick sacrificial layer, as a conservative example, the new architecture can handle droplets of $\sim$100 pL. This represents a 1000-fold reduction in volume compared to droplets in traditional assembled chips. Although it is not experimentally demonstrated in this paper, one could use common micromachining facilities to fabricate electrodes 10 μm on a side with a 2 μm distance between them and a 2 μm-thick sacrificial layer. This would result in a monolithic EWOD chip capable of handling femtoliter droplets.

The ability to handle much smaller droplets will make new applications, such as single-cell analysis, accessible to digital EWOD. Motivated by the recent push from biologists to study heterogeneity within cell populations, various microfluidic platforms have been developed for trapping (e.g., physical microtraps [14], dielectrophoretic (including light induced [15]) traps [16]), and monitoring (e.g., optical [17] or electrical [18]) of single cells and organelles under various stimuli [19]–[23], etc. A promising approach is to create, manipulate, and examine discrete nano- and picoliter liquid volumes containing one or a few cells each [24], [25]. In such platforms, stimuli (e.g., chemical, mechanical, thermal, and electrical) and responses (e.g., secreted chemicals, division, apoptosis) are localized to each droplet, i.e., in an individual reactor, and thus rare cell-type responses are detected—this is in contrast to conventional techniques that mash together cell populations before analyzing the contents, giving output that is spatially and temporally averaged. Cai *et al.* [26] reported isolation and long-term monitoring of protein expression of single cells in 100 pL of liquid. Their chip effectively solved the "efflux" problem, i.e., loss of analyte signal due to rapid diffusion away from the cell, by physically confining the cell and its secretions. He *et al.* [24] integrated optical trapping with a microfluidic T-channel droplet generator, thereby demonstrating a different way to encapsulate single cells and molecules of interest inside pico- and femto-liter droplets. Even among the highly versatile pressure-driven *droplet* microfluidic systems of today that are capable of splitting, mixing, and merging thousands of droplets in parallel [27]; *digital* microfluidic chips (such as the one reported here) bring a distinct set of capabilities such as independent and reconfigurable droplet routing and liquid-in-gas operation, both of which are important for long-term cell culture and monitoring.

Contamination can be an issue when operating EWOD chips, and the processes used for removing residues prior to or between experiments are different for assembled and monolithic devices. For example, it is a common practice in the research setting to assemble chips outside the clean room and risk contamination from the environment. It should be noted that this is less of a concern when oil is used as a filler medium. During experiments, disassembly is often required to clean or recondition the substrate. This can be complicated by the fact that adhesive spacers are generally dissolved by cleaning agents, e.g., organic solvents and sulfuric acid, and need to be replaced. These complications, however, can be avoided by using chemically resistant spacers, e.g., SU-8 or polyimide, that do not need to be replaced during the cleaning process. In any case, the reported monolithic chip fabrication is not subject to contamination from the ambient environment because the chip cavity is created in the clean room. This procedure ensures that there is no initial contamination. Also, the device is relatively impervious to cleaning agents; the only polymers that exist on the chip are Teflon or Cytop, which are exceptionally chemically stable. To clean the monolithic chip between experiments, it was soaked in a solvent (e.g., acetone) and rinsed with water.

Fig. 1 provides a visual comparison of assembled (1a) and monolithic (1b) parallel-plate EWOD devices. With assembled devices intended for actuating droplets in a gas medium, issues associated with assembly (i.e., poor dimensional control, contamination, spacer degradation) are more detrimental to device performance as the gap height is reduced. By eliminating the need for device assembly, monolithic chips can be scaled down very accurately to handle picoliter droplets in air immediately following clean room fabrication. After designing

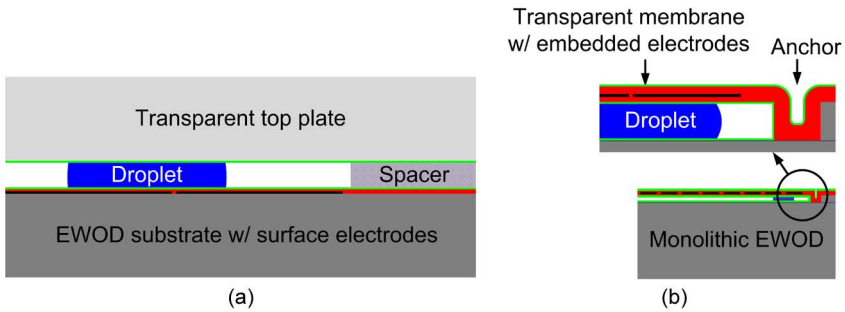

Fig. 1. Schematic comparison of (a) assembled and (b) monolithic EWOD chips.

and fabricating the monolithic EWOD chip, we confirmed its successful operation by demonstrating core digital microfluidic functions: droplet creation, transport, splitting, and merging. We also explored additional microfluidic functions involving droplet flow focusing and particle manipulation.

II. Device Design, Architecture, and Fabrication

A. Fabrication

The monolithic EWOD chip is fabricated by surface micromachining, as shown in Fig. 2. (1) The starting material is a 4″ SOI wafer with a 10 μm-thick device layer, 0.25 μm-thick buried SiO_2, and 525 μm-thick handle layer (resistivity $= 0.01 - 0.02\ \Omega \cdot \mathrm{cm}$). (2) The process begins with photolithographic patterning and deep reactive-ion-etching of the silicon device layer. The recesses etched in this step define the anchors of the eventual membrane. (3) Wet thermal oxidation is used to grow 100 nm of SiO_2 on all exposed silicon. This oxide layer is necessary to protect the membrane from the release etch, discussed later. (4) A 1 μm low-stress silicon nitride (Si_xN_y) layer is deposited by plasma-enhanced chemical vapor deposition (PEVCD). (5) Metals (7/100 nm Ti/Au) are deposited onto the substrate by electron-beam evaporation. (6) The metals are photolithographically patterned and wet etched (Au was etched by commercial gold etchant; Ti was etched by a commercial buffered oxide etchant containing HF) to form electrodes. (7) Another photolithography and wet etch are used to selectively remove Au from electrodes on the membrane, leaving behind the transparent Ti electrodes. Even though the process flow does not show it, Au remains on contact pads and lead wires on the chip. We note that the 7 nm of Ti served as an adhesion layer for the Au as well as a highly transparent and sufficiently conductive layer for EWOD actuation. It was therefore unnecessary to add another layer, e.g., ITO, to form transparent actuation pads. (8) Another low-stress Si_xN_y layer (3 μm thick this time) is deposited by PECVD. (9) The next step (not shown as it is outside the view) is photolithographic patterning and CF_4 plasma etching of the uppermost Si_xN_y layer to uncover electrical contact pads at the edge of each chip on the wafer. (10) Release holes are patterned and etched using CF_4 plasma. (11) The membranes are released by XeF_2 vapor-phase etching, and the cavities are formed. (12) Finally, the chips are spin coated (6000 rpm for 120 s) with a hydrophobic polymer solution (1 wt% Cytop) and baked in an oven at 150 °C for 10 min. The following procedure was used to measure the thickness of the Cytop layer inside the EWOD

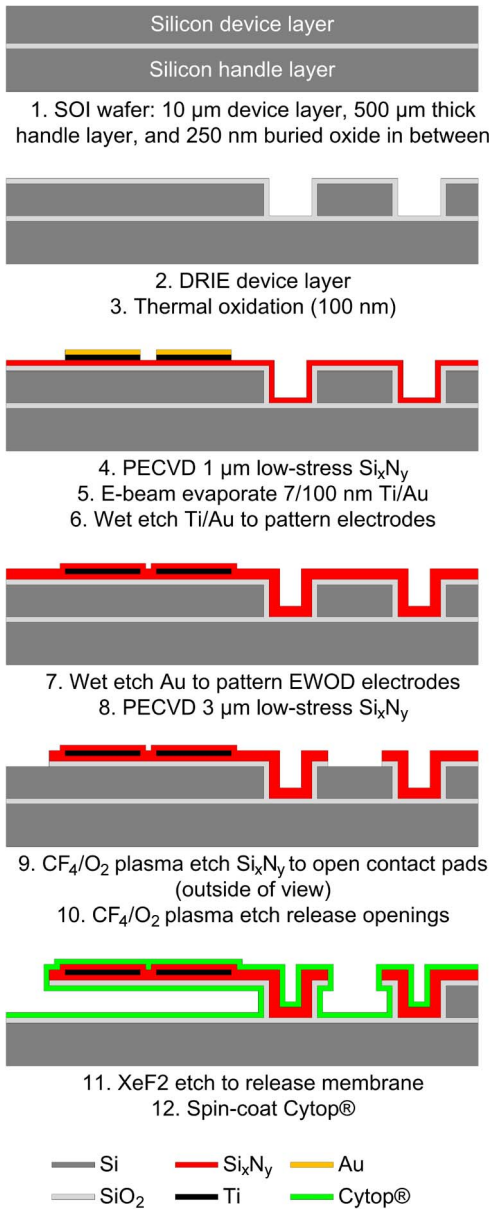

Fig. 2. Process flow to surface micromachine the monolithic EWOD chip.

cavity: (i) membranes were peeled off (using adhesive tape) of experimentally verified chips, (ii) the bottom surface of the cavity was scratched several times using a stainless steel probe tip, (iii) and the area was scanned using a stylus profilometer. For three devices that were spin coated using the same process, the thickness was 38 ± 6.8 nm. For each device, two spots were

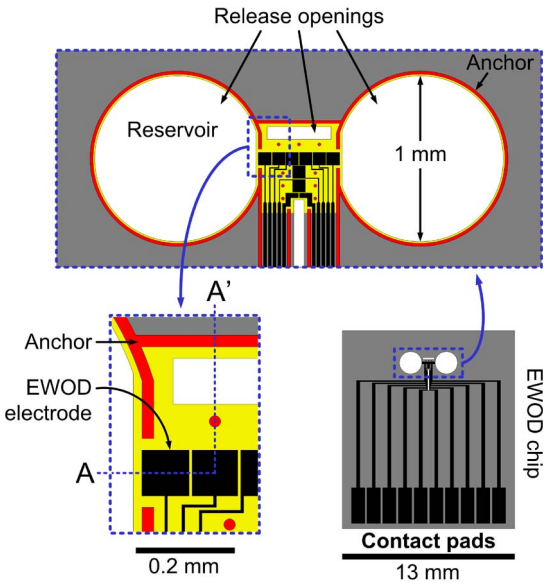

Fig. 3. Layout of a monolithic EWOD chip drawn at three scales, showing the overall chip (lower right), the EWOD electrodes and liquid reservoirs (upper), and the entry point to the EWOD cavity (lower left). The silicon device is colored gray, the electrodes are black, the anchors are red, the release openings are white, and the membrane is yellow. The cross section $A - A'$ corresponds to the fabrication process flow in Fig. 2.

measured inside the cavity—one near the center of the cavity and one near the entrance from the reservoir. We did not observe any tendency in the thickness variation related to measurement location.

In a previous report [13], we characterized the gap height variation attributable to membrane deflections caused by intrinsic stress in the films. We found that, for membranes identical to those reported here, the maximum deflection of a membrane spanning 300 μm was less than 200 nm. This represents an extreme case because anchors need not be so far apart. Even so, such a minor deflection would lead to only a 1.3% uncertainty in droplet volume of a 100 pL droplet (assuming the volume is 100 μm $\times$ 100 μm $\times$ gap height).

B. Architecture

Fig. 3 shows schematic top views of a completed chip consisting of three basic components: anchors, electrodes, and membranes. Anchors are the structural linkages between the substrate and the suspended membrane. Also, anchors serve as etch stops (in the direction parallel to the wafer surface) during the membrane release etch and define the cavity areas. Note that the EWOD electrodes are embedded within the membrane, i.e., within the top plate. Typical assembled parallel-plate EWOD chips have the actuation electrodes on the bottom substrate. Whether the electrodes are in the "top" or "bottom" is not an important distinction given that they are relative terms—the key distinction of the monolithic chip from the assembled chips is that the EWOD dielectric is deposited before the electrodes instead of after. This layer configuration, which happens to produce a perfectly flat actuation surface, was a natural choice after our decision to use the SOI device layer as a sacrificial layer. Release openings in the membrane allow access to the sacrificial layer etchant during the formation of the cavity beneath the membrane. Also, release openings, if placed near or on top of the EWOD electrodes, can serve as liquid source or waste reservoirs during device operation. For example, two large circular release openings (diameter $= 1$ mm) were filled with liquid ($\sim$1 μL each) for most of the device demonstrations described in later sections.

The monolithic architecture used in this study (Fig. 1) utilizes parallel-plate actuation because the handle wafer is electrically grounded, and actuation force is delivered via electrodes embedded in the membrane. As in most parallel-plate systems, the droplet is not actually grounded, but the dielectric covering the grounding plate (the substrate in our case) is very thin compared to that covering the actuation electrodes, so the latter represents the dominant capacitance in the circuit.

C. Scaling of EWOD Forces With Thicknesses of Layers

Surface micromachining enables accurate control of cavity heights in the micrometer range. Digital EWOD devices having gap heights below 100 μm have demonstrated droplet manipulations in oil using an assembled chip with an SU-8 spacer [10]–[12] and in air using a chip mounted to a micrometer to control the gap [28]. Using a similar device configuration, but with a photo-conductive layer rather than patterned electrodes, Chiou *et al.* [29] demonstrated "optoelectrowetting" manipulation of 10 pL droplets. Importantly, in the parallel-plate configuration, all layers of the EWOD device (i.e., liquid, vapor, dielectric, hydrophobic, etc.) have at least some contribution to the overall electrical driving force [30]. In this way, EWOD differs from driving mechanisms based on thermally or chemically induced wettability gradients, which have also been employed in digital microfluidic systems [31]–[33]. As a reference for surface force-based droplet actuation, we recommend the review of Darhuber and Troian [34]. To illustrate the importance of the entire EWOD circuit, in which electrodes, insulators, and fluids are represented by electrical components, we use the electromechanical model developed by Jones *et al.* [35]. The following simplified analysis shows how the variation of EWOD forces with actuation frequency is dependent on the ratio of cavity height h to dielectric thickness d. It is important to note that in most cases, the electrowetting force equation is developed with the assumption that $h \gg d$, leading to the result that the time-averaged force parallel to the direction of motion is $F = 0.5cV^2$, where the specific capacitance c is only a function of d. The following analysis, however, does not assume $h \gg d$ because our intention is to show how the total electrical force changes when h is scaled down to dimensions similar to d. Using the circuit model shown in Fig. 4(a), we express the dimensionless voltage drops (divided by the applied voltage V) across the liquid (subscript "1") and dielectric (subscript "2") layers as

$$\frac{V_{1,\text{liquid}}}{V} = \left| \frac{1}{1 + \frac{d}{h}\left(\frac{\varepsilon_1}{\varepsilon_2} - j\frac{\sigma}{\omega\varepsilon_2}\right)} \right| ; \quad \frac{V_{1,\text{vapor}}}{V} = \frac{1}{1 + \frac{\varepsilon_v}{\varepsilon_2}\frac{d}{h}} \tag{1a}$$

$$\frac{V_{2,\text{wet}}}{V} = \left| \frac{\frac{d}{h}\left(\frac{\varepsilon_1}{\varepsilon_2} - j\frac{\sigma}{\omega\varepsilon_2}\right)}{1 + \frac{d}{h}\left(\frac{\varepsilon_1}{\varepsilon_2} - j\frac{\sigma}{\omega\varepsilon_2}\right)} \right| ; \quad \frac{V_{2,\text{dry}}}{V} = \frac{1}{1 + \frac{\varepsilon_2}{\varepsilon_v}\frac{h}{d}} \tag{1b}$$

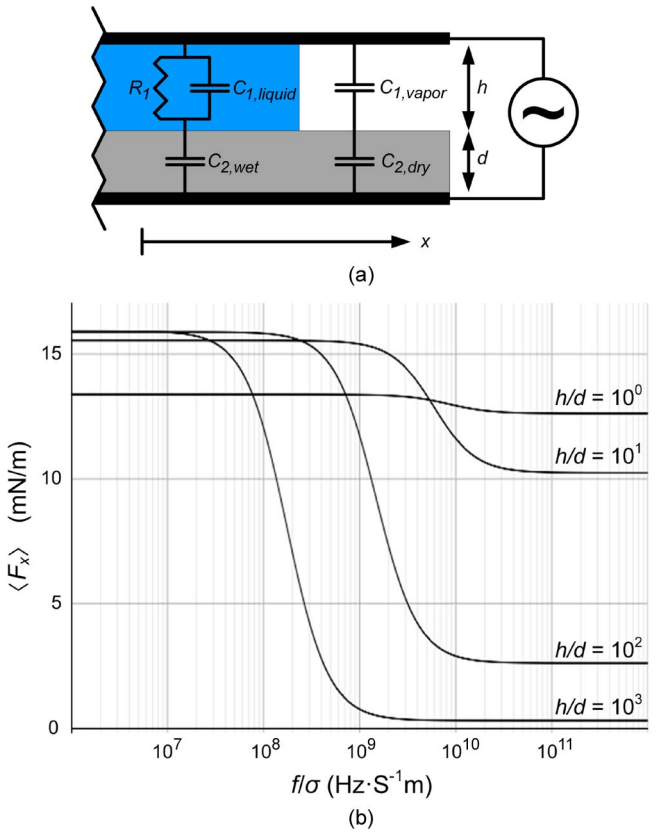

Fig. 4. Scaling of EWOD forces with ratio of cavity height h to dielectric thickness d. (a) Circuit model of electromechanical actuator resembling an EWOD device, and (b) corresponding plot showing time-averaged force per unit length in the x-direction versus f/σ, where f is frequency of actuation voltage and σ is liquid conductivity. Each curve represents a different ratio h/d.

where ε_1 and ε_2 are dielectric constants of liquid and dielectric, respectively, and σ is the liquid conductivity. Referring to Fig. 4(a): Equation (1a) correspond to the voltage across the liquid, which is modeled as a resistor and capacitor with ε_1 (=80 for water) in parallel and the voltage drop across the vapor layer, which is modeled as a capacitor with ε_v (=1, assuming similar to vacuum); Equation (1b) correspond to the voltage drop across the dielectric beneath the liquid and the vapor, which is modeled as a capacitor with ε_2 (=4 for silicon nitride). Using lumped elements, the time-averaged force per unit width (into the page) moving the liquid from left to right is [36]

$$\langle F_x \rangle = \frac{1}{2h}\left(\varepsilon_1 V_{1,\text{liquid}}^2 - \varepsilon_v V_{1,\text{vapor}}^2\right) + \frac{\varepsilon_2}{2d}\left(V_{2,\text{wet}}^2 - V_{2,\text{dry}}^2\right). \tag{2}$$

In Fig. 4(b), the above force is plotted in terms of $\langle F_x \rangle$ versus f/σ, where f is the actuation frequency. Four curves corresponding to different values of h/d ($d = 1$ μm assumed in all cases) show that this ratio affects the actuation force in three ways: (i) decreasing h/d decreases the force at low frequency, (ii) decreasing h/d delays the transition from the low- to high-frequency limits. In order words, if we define a crossover frequency as the inflection point of the force curve, then decreasing h/d increases the crossover frequency, and (iii) decreasing h/d increases the force at high frequency. From Fig. 4(b) and (ii) and (iii) above, we can make a useful conclusion in designing EWOD chips: scaling down of h/d can be a way to lower the actuation voltage when working with low-conductivity liquids (e.g., oils) or at high actuation frequencies.

To keep the model simple, we have left several dielectric layers (e.g., hydrophobic coatings and thermal oxides) out of the circuit. Refer to Chatterjee *et al.* [30] for an excellent demonstration of how to incorporate all layers on the parallel-plate EWOD chip. The model used here is sufficient to show the scaling behavior of h/d, and even without the thin dielectrics, it is reasonably accurate because the capacitances of the thick dielectric and fluid layers are dominant.

We conclude our discussion on the scaling of EWOD forces with a few comments on the fluid dynamics. First, the Reynolds number scales directly with the gap h. A high-speed camera (Phantom v7.2) was used to measure a droplet speed of 100 mm/s at 60 V_{rms} (20 kHz) in the current monolithic chip, which has $h \sim 10$ μm. This is similar to the droplet speed in a typical assembled chip of $h \sim 100$ μm (e.g., [37]), except that the associated Reynolds number is 10 times lower in the monolithic chip. Secondly, if particles are suspended within the liquid, and the gap h is only slightly larger than the particles, then they can move in only one or two dimensions. The second point is demonstrated by our flow focusing experiment discussed in the next section. The ability to scale the microfluidic chip with biological particles such as cells can greatly simplify processes such as inspection and sorting of the particles.

III. Experimental Setup and Procedure

A. Experimental Setup

The experimental setup is shown in Fig. 5. A function generator (Agilent 32200A) outputs a sinusoidal waveform to the voltage amplifier (TREK PZD700A), which outputs the actuation voltages to a homemade electrical multiplexer having a manually operated array of 10 SPDT Submini lever switches (RadioShack). The multiplexer routes voltages to ten addressable channels via a ribbon cable [(3M round conductor flat cable with 1 mm spacing between the wires (28 AWG))] connected to the 34-pin clip holding the EWOD chip. The 34-pin clip, a modified parallel port plug, provides both electrical connections and mechanical clamping to the chip during operation, so no other clamps are necessary. The manual multiplexer was suitable in this study because the tested EWOD devices had ten or less electrodes, many more of which would have required an automated multiplexer. Videos of EWOD operations were captured using two different cameras, depending on the required frame rate (note that the camera in Fig. 5 represents either a normal USB CMOS camera or a high-speed camera). For most observations, we recorded at 30 frames per second using a USB digital camera (Edmund Optics CMOS EO-0413C, 752 × 480 pixels) mounted to an optical microscope (20× objective) on a vibration isolation table. For measuring droplet speeds and tracking the movements of beads inside of droplets, we recorded at 4000 frames per second using a Phantom v7.2 high speed camera (Vision Research). The setup shown in Fig. 5 allowed open access to the chip for pipette sample loading and extraction. In the picture in Fig. 5, the microcavity with

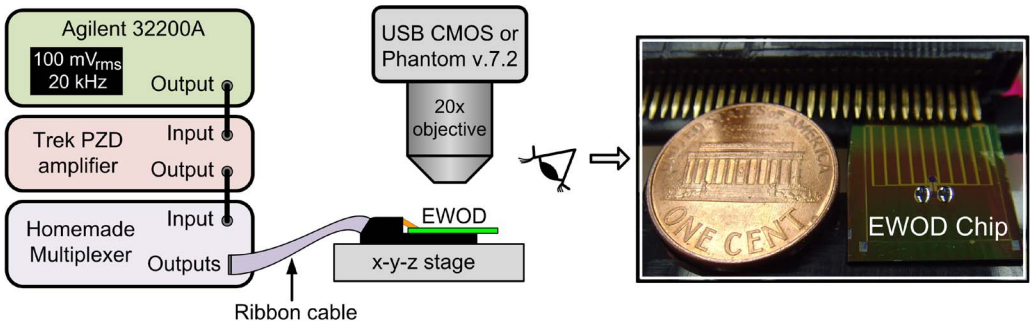

Fig. 5. Experimental setup and picture of monolithic chip (equivalent to the lower right figure of Fig. 3) inserted into the chip holder next to a U.S. penny. The chip is loaded with a large water drop in each of the two circular reservoirs.

EWOD electrodes (too small to see) is located between the two reservoir droplets, which are about 1 mm in diameter.

B. Evaporation of Droplets

Evaporation is an important issue for the monolithic EWOD device because droplets have extremely small volumes. In preparation for EWOD testing, we evaluated the evaporation of water droplets and explored conditions that minimized or eliminated the volume loss. In the current chip designs (similar layouts as Fig. 3), the cavity area is relatively small, and the EWOD electrodes are close to the cavity openings, so the droplets are expected to evaporate nearly as fast as outside the cavity. With all the release openings clear, for instance, a 100 pL water droplet inside the cavity was observed to evaporate completely in about 10 s. However, with full reservoirs, a 100 pL water droplet lasted more than 5 min (versus 10 s) in different devices, where the cavity was designed much deeper and the release openings smaller. In the same condition, a 100 pL 50 : 50 mix of water and glycerol showed no signs of evaporation in 10 min. When a large ($\sim$10 μL) liquid droplet was placed on the device to block all the openings, a 100 pL water droplet inside the cavity showed no signs of evaporation over several hours, suggesting the cavity was saturated with water vapor. The latter condition was used to verify droplet-in-vapor operations shown in Figs. 7–10. As expected, when the cavity was filled with oil [8], no volume loss of water droplet was observed over hours of experimentation.

C. Initial Loading

In a preliminary report in which droplets were actuated only in oil [13], we demonstrated that monolithic EWOD chips could be loaded with liquids via NanoPorts (Upchurch Scientific), which are used commonly in microfluidic devices as micro-to-macro interfaces, i.e., mating microchip inlets/outlets with millimeter-scale tubing. In [13], we used a syringe to pump liquids through tubes connected to the NanoPorts, which were bonded to the chip. The use of NanoPorts with the monolithic device, however, was only meant to prove the EWOD core functions (creation, transport, and splitting) in the surface-micromachined cavity. In this report, the device was designed for loading without NanoPorts. Specifically, with the current chip, liquids are pipetted directly onto the reservoirs, which are defined by release openings next to the EWOD cavity.

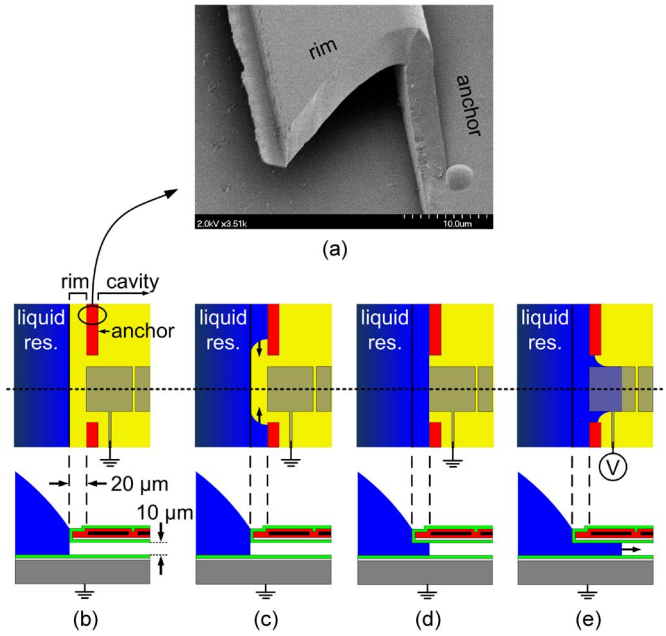

Fig. 6. (a) SEM of the anchor and the rim, which have been intentionally broken to show the vertical wall and the space under the overhang. The viewing angle is 45°. (b)–(e) Schematic illustration of the initial loading. The sequence shows the process of filling the rim around the reservoir: (b) dry, (c) partially filled, (d) fully filled, and (e) loading into the cavity by EWOD actuation.

This method enables straightforward loading of nonwetting liquids (contact angle $> 90°$), because they could be deposited onto the reservoirs without flooding the entire chip. Controlled loading of wetting fluids, e.g., organic solvents or oils, on the hydrophobic Cytop surfaces require another method, e.g., the NanoPort.

Fig. 6 shows a subtle, yet important, detail of chip loading: filling the rim around the reservoir with a nonwetting liquid, e.g., water. For the liquid to be accessible to the EWOD electrodes, it must first occupy the space beneath a rim of membrane that surrounds the reservoir, as shown in Fig. 6(a). When a droplet is first loaded [Fig. 6(b)], the region beneath the rim is dry. To fill, or prime, the reservoir [Fig. 6(c) and (d)], we deposited a warm water droplet onto the chip. This led to condensation within the rim region and complete filling in several seconds. Once primed [Fig. 6(e)], the chip could be filled with any liquid and operated. Various design modifications will eliminate this priming step in the future, such as using an EWOD electrode that extends into the rim of the membrane

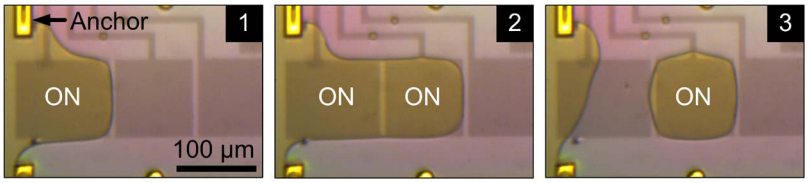

Fig. 7. Video frames (seen through the top membrane) of introducing water into the cavity and creating a 100 pL droplet ($100\ \mu\text{m} \times 100\ \mu\text{m} \times 10\ \mu\text{m}$) using 60 V_{rms} at 20 kHz. The liquid is under the electrodes, which are imbedded in the transparent membrane. Actuated electrodes are labeled "ON," and all other electrodes as well as the substrate silicon are grounded. The two small droplets on the electrode wires above the actuation electrodes are satellite droplets formed unintentionally during previous actuations. Anchors appear yellow because gold remained (harmlessly) in the 10 μm-deep recesses after the lithography.

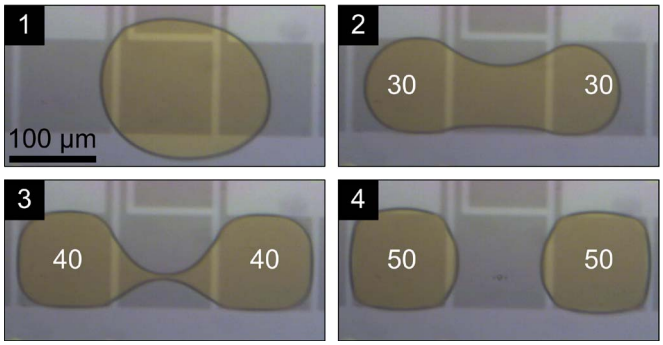

Fig. 8. Video frames (seen through the top membrane) of incremental droplet splitting using 30, 40, and 50 V_{rms} at 20 kHz. Each voltage was applied continuously and raised by 10 V every 3–4 s. The droplet immediately broke apart at the application of 50 V_{rms}.

and/or reducing the width of the rim itself such that EWOD forces pull liquid directly from the reservoir.

IV. Results and Discussion

A. Creation and Splitting of Droplets

The core digital microfluidic functions of droplet creation, transport, splitting, and merging [4] were demonstrated using the monolithic EWOD chip. Fig. 7 is a sequence of video frames showing creation of deionized water droplets in air (saturated with water vapor) inside the microcavity using 60 V_{rms} at 20 kHz for EWOD actuation. While droplet transport was repeatable at voltages down to 30 V_{rms}, creation was not repeatable below 60 V_{rms}. Similarly, droplet splitting required voltages greater than 50 V_{rms} to be repeatable. Fig. 8 is a sequence of video frames showing the shape of a droplet at various voltages too low to cause splitting. The voltage was applied continuously and increased by 10 V every 3–4 s. At 30 V_{rms} the droplet begins to neck, at 40 V_{rms} the neck becomes much thinner, and the droplet breaks immediately upon increasing the voltage to 50 V_{rms}. We tested a range of actuation frequencies (up to 50 kHz) and found that actuation was most reliable at 10 to 20 kHz. Also, the transportation of droplets with 30 V_{rms} was successful at $f < 30$ kHz but not at higher frequencies (tested up to 50 kHz). This behavior could be a result of the redistribution of electric field and concomitant decrease in actuation force [as seen in [30] and indicated by the curves in Fig. 4(b)]. For example, in Fig. 4(b), the curve for $h/d = 10$, roughly representing the current fabrication, sustains its maximum value up to $f/\sigma \sim 5 \times 10^8$ before decreasing. Using the conductivity of deionized water after exposure to air reported in [38] ($\sigma \sim 7 \times 10^{-5}$ S/m), we calculate the critical frequency to be $f = 35$ kHz, which agrees with our observation.

B. Flow Focusing and Particle Manipulation

In exploring the utilities of the surface-micromachined EWOD chip, we have tested flow focusing of droplets suspended with particles. With the reported fabrication process, it is simple to incorporate arbitrarily shaped posts or walls in the EWOD cavity at many locations. It is also important to note that such structures are perfectly sealed to the upper and lower inner surfaces of the cavity. This is a consequence of the fact that the vertical structures (anchors) and membrane(s) are made of the same structural layer. It is possible to build constrictions through which droplets can be squeezed by EWOD actuation, thereby accomplishing flow focusing. By flow focusing, we are referring the process by which liquid and suspended particles are forced through an orifice to increase the sensitivity of a measurement, e.g., electrical impedance [39]. Note that flow focusing also refers to the process by which liquid streams are pinched such that they break up into droplets [40]. Fig. 9 is a sequence of video frames showing the creation, transport, and flow focusing of a droplet through a 40 μm wide constriction defined by the two constriction anchors. Flow focusing is often used in microchannels either by physical constrictions or sheath flows to analyze particles one-by-one, e.g., microfluidic cytometry [41].

Dhindsa *et al.* [42] recently reported an interesting EWOD configuration in which liquid is actuated through arrays of microposts, thereby creating $\sim 20 \times 20\ \mu$m virtual microchannels of water in oil. This type of flow constriction is similar to that shown here, except the monolithic chip has digitized electrodes for handling individual droplets. Fig. 10 shows examples of focusing droplets containing twelve [Fig. 10(a)] and one [Fig. 10(b)] polystyrene beads (Invitrogen, Surfactant-Free Fluorescent Nile Red CML Polystyrene Latex, Product No: 2-FN-5000, diameter $= 5.3\ \mu$m). Note the bead diameter is more than a half of the cavity height, rendering particle movements nearly 2-D. To track the path of the particles through the constriction, it was necessary to use a high-speed camera, recording at 4000 frames per second. Fig. 10(c) is a composite image showing the initial meniscus of a droplet (broken line) and final meniscus after 2.5 ms into the focusing actuation (solid line). Also, shown are the locations of the particle at 0.25 ms intervals, which are connected by a blue line to show its path through the constriction.

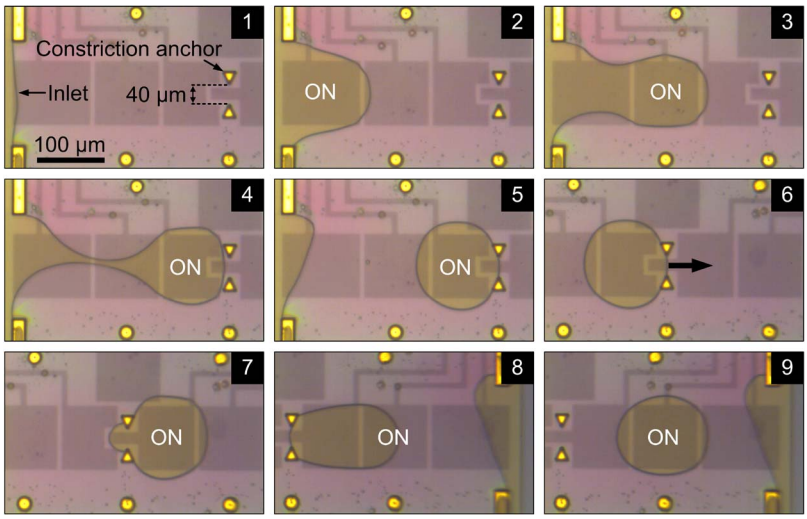

Fig. 9. Video frame sequence of droplet flow focusing. Between steps 6 and 7, the water droplet is squeezed between the 40 μm wide constriction formed by two triangular anchors located between two EWOD electrodes.

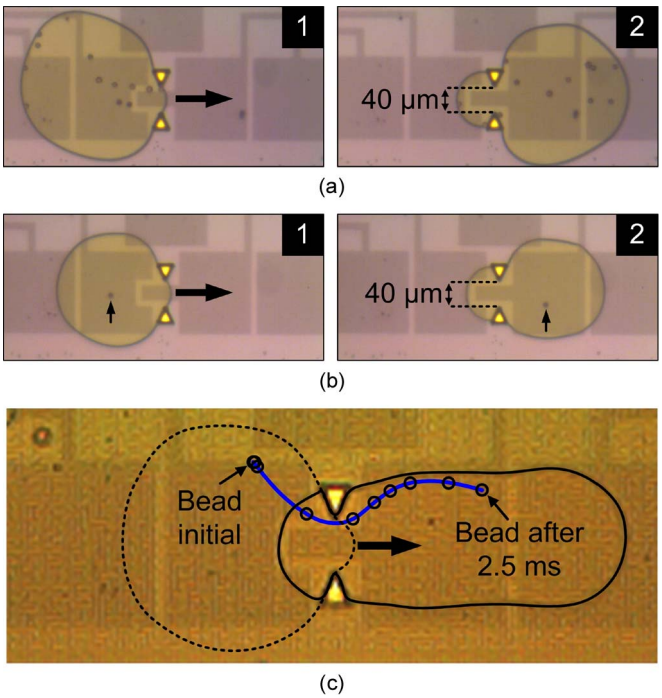

Fig. 10. Video frames of droplet flow focusing and particle handling. Large black arrows indicate the direction of droplet motion. (a) A droplet containing twelve 5.3 μm beads before (1) and after (2) moving through the constriction. (b) A droplet containing one 5.3 μm bead before (1) and after (2) moving through the constriction. (c) A composite image created using high-speed video frames of focusing a droplet containing one 5.3 μm bead. Lines were drawn over menisci at $t = 0$ (dashed black line) and $t = 2.5$ ms (solid black line). Bead locations at 0.25 ms intervals are shown by black circles, which are connected by a blue line to show the bead path.

In the reported chip, a 100 pL ($100\ \mu\text{m} \times 100\ \mu\text{m} \times 10\ \mu\text{m}$) droplet containing a single 5.3 μm bead was created as follows. First, a droplet was created from a reservoir of liquid containing the beads. If the initial droplet happened to contain several beads, a series of splitting and merging operations were performed to render a droplet containing only one bead. The number of beads within the initial droplet was dependent upon the concentration of beads in the reservoir. We have not fully characterized this relationship, but with roughly 3×10^5 beads/mL, initial droplets contained one to five beads.

V. Conclusion

Surface micromachining has been developed to fabricate monolithic EWOD chip on a single wafer, requiring no post-processing or assembly to obtain the parallel-plate configuration. The monolithic architecture used a thin-film membrane with embedded actuation electrodes as the top plate instead of a second substrate, as is necessary for assembled EWOD chips. The new process enables unprecedented dimensional control in the fabrication of parallel-plate EWOD devices. Reported devices have gap heights of 10 μm with 0.5 μm accuracy across the entire wafer. The core digital microfluidic functions (creation, transport, and splitting) as well as advanced functions (flow focusing of droplets with suspended particles) have been demonstrated using 100 pL water droplets in air inside a 10 μm-high microcavity.

References

[1] G. M. Whitesides, "The origins and future of microfluidics," *Nature*, vol. 442, no. 7101, pp. 368–373, Jul. 2006.
[2] R. B. Fair, "Digital microfluidics: Is a true lab-on-a-chip possible?" *Microfluid. Nanofluid.*, vol. 3, no. 3, pp. 245–281, Jun. 2007.
[3] W. C. Nelson and C.-J. Kim, "Droplet actuation by electrowetting-on-dielectric (EWOD): A review," *J. Adhes. Sci. Technol.—Special Issue on Electrowetting*, to be published.
[4] J. Lee, "Microactuation by continuous electrowetting and electrowetting: Theory, fabrication, and demonstration," Ph.D. dissertation, Univ. California, Los Angeles, CA, 2000.
[5] J. Gong, S.-K. Fan, and C.-J. Kim, "Portabile digital microfluidics platform with active but disposable lab-on-chip," in *Proc. IEEE Int. Conf. MEMS*, Maastricht, The Netherlands, Jan. 2004, pp. 355–358.
[6] M. G. Pollack, R. B. Fair, and A. D. Shenderov, "Electrowetting-based actuation of liquid droplets for microfluidic applications," *Appl. Phys. Lett.*, vol. 77, no. 11, pp. 1725–1726, Sep. 2000.
[7] S. K. Cho, H. Moon, and C.-J. Kim, "Creating, transporting, cutting, and merging liquid droplets by electrowetting-based actuation for digital microfluidic circuits," *J. Microelectromech. Syst.*, vol. 12, no. 1, pp. 70–80, Feb. 2003.
[8] U.-C. Yi and C.-J. Kim, "Characterization of electrowetting actuation on addressable single-side coplanar electrodes," *J. Micromech. Microeng.*, vol. 16, no. 10, pp. 2053–2059, Oct. 2006.

[9] C. G. Cooney, C. Y. Chen, M. R. Emerling, A. Nadim, and J. Sterling, "Electrowetting droplet microfluidics on a single planar surface," *Microfluid. Nanofluid.*, vol. 2, no. 5, pp. 435–446, 2006.
[10] J. H. Song, R. Evans, Y.-Y. Lin, B.-N. Hsu, and R. B. Fair, "A scaling model for electrowetting-on-dielectric microfluidic actuators," *Microfluid. Nanofluid.*, vol. 7, no. 1, pp. 75–89, Jul. 2009.
[11] Y.-Y. Lin, R. D. Evans, E. Welch, B.-N. Hsu, A. C. Madison, and R. B. Fair, "Low voltage electrowetting-on-dielectric platform using multi-layer insulators," *Sens. Actuators B, Chem.*, vol. 150, no. 1, pp. 465–470, Sep. 2010.
[12] E. R. F. Welch, Y.-Y. Lin, A. Madison, and R. B. Fair, "Picoliter DNA sequencing chemistry on an electrowetting-based digital microfluidic platform," *Biotechnol. J.*, vol. 6, no. 2, pp. 165–176, Feb. 2011.
[13] W. C. Nelson and C.-J. Kim, "A monolithic EWOD chip by surface micromachining," in *Proc. Solid-State Sens., Actuator Microsyst. Workshop, Tech. Dig.*, Hilton Head Island, SC, Jun. 2010, pp. 158–161.
[14] D. DiCarlo, L. Y. Wu, and L. P. Lee, "Dynamic single cell culture array," *Lab Chip*, vol. 6, no. 11, pp. 1445–1449, 2006.
[15] P. Y. Chiou, A. T. Ohta, and M. C. Wu, "Massively parallel manipulation of single cells and microparticles using optical images," *Nature*, vol. 436, no. 7049, pp. 370–372, Jul. 2005.
[16] J. Voldman, M. L. Gray, M. Toner, and M. A. Schmidt, "A microfabrication-based dynamic array cytometer," *Anal. Chem.*, vol. 74, no. 16, pp. 3984–3990, Aug. 2002.
[17] A. R. Wheeler, W. R. Throndset, R. J. Whelan, A. M. Leach, R. N. Zare, Y. H. Liao, K. Farrell, I. D. Manger, and A. Daridon, "Microfluidic device for single-cell analysis," *Anal. Chem.*, vol. 75, no. 14, pp. 3581–3586, Jul. 2003.
[18] A. A. Werdich, E. A. Lima, B. Ivanov, I. Ges, M. E. Anderson, J. P. Wikswo, and F. J. Baudenbacher, "A microfluidic device to confine a single cardiac myocyte in a sub-nanoliter volume on planar microelectrodes for extracellular potential recordings," *Lab Chip*, vol. 4, pp. 357–362, 2004.
[19] D. DiCarlo and L. P. Lee, "Dynamic single-cell analysis for quantitative biology," *Anal. Chem.*, vol. 78, no. 23, pp. 7918–7925, Dec. 2006.
[20] M. Leslie, "The power of one," *Science*, vol. 331, no. 6013, pp. 24–26, Jan. 2011.
[21] D. T. Chiu and R. M. Lorenz, "Chemistry and biology in femtoliter and picoliter volume droplets," *Acc. Chem. Res.*, vol. 42, no. 5, pp. 649–658, May 2009.
[22] R. N. Zare and S. Kim, "Microfluidic platforms for single-cell analysis," *Annu. Rev. Biomed. Eng.*, vol. 12, pp. 187–201, 2010.
[23] H. Wu, A. R. Wheeler, and R. N. Zare, "Chemical cytometry on a picoliter-scale integrated microfluidic chip," *Proc. Nat. Acad. Sci. U.S.A.*, vol. 101, no. 35, pp. 12 809–12 813, Aug. 2004.
[24] M. He, J. S. Edgar, G. D. M. Jeffries, R. M. Lorenz, J. P. Shelby, and D. T. Chiu, "Selective encapsulation of single cells and subcellular organelles into picoliter- and femtoliter-volume droplets," *Anal. Chem.*, vol. 77, no. 6, pp. 1539–1544, Mar. 2005.
[25] D. Irimia, R. G. Tompkins, and M. Toner, "Single-cell chemical lysis in picoliter-scale closed volumes using a microfabricated device," *Anal. Chem.*, vol. 76, no. 20, pp. 6137–6143, Oct. 2004.
[26] L. Cai, N. Friedman, and S. Xie, "Stochastic protein expression in individual cells at the single molecule level," *Nature*, vol. 440, no. 7082, pp. 358–362, Mar. 2006.
[27] S.-Y. Teh, R. Lin, L.-H. Hung, and A. P. Lee, "Droplet microfluidics," *Lab Chip*, vol. 8, no. 2, pp. 198–220, 2008.
[28] S. U. Son, D. Chatterjee, and R. L. Garrell, "Electrically-induced splitting and generation of sub-nanoliter droplets in air on a digital microfluidic device," in *Proc. Int. Conf. μTAS*, Tokyo, Japan, 2006, pp. 128–130.
[29] P. Y. Chiou, S.-Y. Park, and M. C. Wu, "Continuous optoelectrowetting for picoliter droplet manipulation," *Appl. Phys. Lett.*, vol. 93, no. 22, pp. 221 110-1–221 110-3, Dec. 2008.
[30] D. Chatterjee, H. Shepherd, and R. L. Garrell, "Electromechanical model for actuating liquids in a two-plate droplet microfluidic device," *Lab Chip*, vol. 9, no. 9, pp. 1219–1229, 2009.
[31] T. S. Sammarco and M. A. Burns, "Thermocapillary pumping of discrete drops in microfabricated analysis devices," *AIChE J.*, vol. 45, no. 2, pp. 350–366, Feb. 1999.
[32] M. K. Chaudhury and G. M. Whitesides, "How to make water run uphill," *Science*, vol. 256, no. 5063, pp. 1539–1541, Jun. 1992.
[33] N. L. Abbott and G. M. Whitesides, "Potential-dependent wetting of aqueous solutions on self-assembled monolayers formed from 15-(ferrocenylcarbony1)pentadecanethiol on gold," *Langmuir*, vol. 10, pp. 1493–1497, 1994.
[34] A. A. Darhuber and S. M. Troian, "Principles of microfluidic actuation by modulation of surface stresses," *Annu. Rev. Fluid Mech.*, vol. 37, pp. 425–455, 2005.
[35] T. B. Jones, J. D. Fowler, Y. S. Chang, and C.-J. Kim, "Frequency-based relationship of electrowetting and dielectrophoretic liquid microactuation," *Langmuir*, vol. 19, pp. 7646–7651, 2003.
[36] T. B. Jones and K.-L. Wang, "Frequency-dependent electromechanics of aqueous liquids: Electrowetting and dielectrophoresis," *Langmuir*, vol. 20, pp. 2813–2818, 2004.
[37] H. Ren, R. B. Fair, M. G. Pollack, and E. J. Shaughnessy, "Dynamics of electro-wetting droplet transport," *Sens. Actuators B, Chem.*, vol. 87, no. 1, pp. 201–206, Nov. 2002.
[38] R. M. Pashley, M. Rzechowicz, L. R. Pashley, and M. J. Francis, "Degassed water is a better cleaning agent," *J. Phys. Chem. B*, vol. 109, no. 3, pp. 1231–1238, Jan. 2005.
[39] T. Sun and H. Morgan, "Single-cell microfluidic impedance cytometry: A review," *Microfluid. Nanofluid.*, vol. 8, no. 4, pp. 423–443, Apr. 2010.
[40] T. Ward, M. Faivre, M. Abkarian, and H. A. Stone, "Microfluidic flow focusing: Drop size and scaling in pressure versus flow-rate-driven pumping," *Electrophoresis*, vol. 26, no. 19, pp. 3716–3724, Oct. 2005.
[41] M. A. McClain, C. T. Culbertson, S. C. Jacobson, and J. M. Ramsey, "Flow cytometry of *Escherichia coli* on microfluidic devices," *Anal. Chem.*, vol. 73, no. 21, pp. 5334–5338, Nov. 2001.
[42] M. Dhindsa, J. Heikenfeld, S. Kwon, S. Park, J. Park, P. D. Rack, and I. Papautsky, "Virtual electrowetting channels: Electronic liquid transport with continuous channel functionality," *Lab Chip*, vol. 10, no. 7, pp. 832–836, 2010.

Wyatt C. Nelson was born in Seattle, WA, in 1983. He received the B.S. degree in mechanical engineering from Cornell University, Ithaca, NY, in 2006, and the Ph.D. degree in mechanical engineering from the University of California at Los Angeles (UCLA), in 2011.

He is currently with the Micro and Nano Manufacturing Laboratory at UCLA. His research interests include digital microfluidics and electrowetting-on-dielectric.

Chang-Jin "CJ" Kim (S'89–M'91) received the B.S. degree from Seoul National University, Seoul, Korea, the M.S. degree from Iowa State University, Ames, and the Ph.D. degree from the University of California, Berkeley, in 1991, all in mechanical engineering.

Since joining the faculty at the University of California at Los Angeles (UCLA), in 1993, he has developed several microelectromechanical systems (MEMS) courses and established a MEMS Ph.D. major field in the Mechanical and Aerospace Engineering Department in 1997. Directing the Micro and Nano Manufacturing Laboratory, he is also a founding member of the California NanoSystems Institute at UCLA. His research interests are in MEMS and nanotechnology, including design and fabrication of micro/nano structures, actuators, and systems, with a focus on the use of surface tension.

Prof. Kim has served on numerous technical committees and panels, including Transducers, the IEEE International Conference on MEMS, and the National Academies Panel on Benchmarking the Research Competitiveness of the U.S. in Mechanical Engineering. He is currently serving on the Editorial Advisory Board for the *IEEJ Transactions on Electrical and Electronic Engineering* and on the Editorial Board for the *Journal of Microelectromechanical Systems*. An ASME Fellow, he was the recipient of the Graduate Research Excellence Award from Iowa State University, the 1995 TRW Outstanding Young Teacher Award, a 1997 NSF CAREER Award, the 2002 ALA Achievement Award, and the 2008 Samueli Outstanding Teaching Award. He has also been active in the commercial sector as a board member, scientific advisor, consultant, and founder of start-up companies.